AUTHOR QUERY FORM

ELSEVIER	Journal: RSE Article Number: 8063	Please e-mail or fax your responses and any corrections to: E-mail: corrections.esil@elsevier.spitech.com Fax: +1 619 699 6721

Dear Author,

Any queries or remarks that have arisen during the processing of your manuscript are listed below and highlighted by flags in the proof. Please check your proof carefully and mark all corrections at the appropriate place in the proof (e.g., by using on-screen annotation in the PDF file) or compile them in a separate list.

For correction or revision of any artwork, please consult http://www.elsevier.com/artworkinstructions.

Any queries or remarks that have arisen during the processing of your manuscript are listed below and highlighted by flags in the proof. Click on the 'Q' link to go to the location in the proof.

Location in article	Query / Remark: click on the Q link to go Please insert your reply or correction at the corresponding line in the proof
Q1	Please confirm that given names and surnames have been identified correctly.
Q2	The citation "Wahr et al., 1988" has been changed to match the author name/date in the reference list. Please check and correct if necessary.
Q3	Citation "Bamber, 1994" has not been found in the reference list. Please supply full details for this reference.
Q4	Citation "Frappart et al., 2006" has not been found in the reference list. Please supply full details for this reference.
Q5	The citation "Bwangoy et al., 2010" has been changed to match the author name/date in the reference list. Please check and correct if necessary.

Thank you for your assistance.

Remote Sensing of Environment xxx (2011) xxx

Contents lists available at SciVerse ScienceDirect

Remote Sensing of Environment

journal homepage: www.elsevier.com/locate/rse

Highlights

Remote Sensing of Environment xxx (2011) xxx–xxx

Characterization of terrestrial water dynamics in the Congo Basin using GRACE and satellite radar altimetry

Hyongki Lee [a,b,*], R. Edward Beighley [c], Douglas Alsdorf [a,b], Hahn Chul Jung [d], C.K. Shum [a,b], Jianbin Duan [a], Junyi Guo [a], Dai Yamazaki [e], Konstantinos Andreadis [b]

[a] *School of Earth Sciences, The Ohio State University, Columbus, OH, USA*
[b] *Byrd Polar Research Center, The Ohio State University, Columbus, OH, USA*
[c] *Civil, Construction and Environmental Engineering, San Diego State University, San Diego, CA, USA*
[d] *NASA Goddard Space Flight Center, Greenbelt, MA, USA*
[e] *Department of Civil Engineering, University of Tokyo, Tokyo, Japan*

► We provide the first-ever measurements of the Congo wetlands water volume change. ► Wetland water is dominated by local upland runoff and much less from mainstem. ► Differences between the Congo wetland and the Amazon floodplain are highlighted.

0034-4257/$ – see front matter © 2011 Published by Elsevier Inc.
doi:10.1016/j.rse.2011.08.015

RSE-08063; No of Pages 9

Remote Sensing of Environment xxx (2011) xxx–xxx

Contents lists available at SciVerse ScienceDirect

Remote Sensing of Environment

journal homepage: www.elsevier.com/locate/rse

Characterization of terrestrial water dynamics in the Congo Basin using GRACE and satellite radar altimetry

Q1 Hyongki Lee [a,b,*,1], R. Edward Beighley [c], Douglas Alsdorf [a,b], Hahn Chul Jung [d], C.K. Shum [a,b], Jianbin Duan [a], Junyi Guo [a], Dai Yamazaki [e], Konstantinos Andreadis [b,2]

[a] School of Earth Sciences, The Ohio State University, Columbus, OH, USA
[b] Byrd Polar Research Center, The Ohio State University, Columbus, OH, USA
[c] Civil, Construction and Environmental Engineering, San Diego State University, San Diego, CA, USA
[d] NASA Goddard Space Flight Center, Greenbelt, MA, USA
[e] Department of Civil Engineering, University of Tokyo, Tokyo, Japan

ARTICLE INFO

Article history:
Received 19 February 2011
Received in revised form 16 June 2011
Accepted 22 August 2011
Available online xxxx

Keywords:
Congo
Wetland
Water storage
GRACE
Satellite Radar Altimetry

ABSTRACT

The Congo Basin is the world's third largest in size (~3.7 million km^2), and second only to the Amazon River in discharge (~40,200 m^3 s^{-1} annual average). However, the hydrological dynamics of seasonally flooded wetlands and floodplains remains poorly quantified. Here, we separate the Congo wetland into four 3°×3° regions, and use remote sensing measurements (i.e., GRACE, satellite radar altimeter, GPCP, JERS-1, SRTM, and MODIS) to estimate the amounts of water filling and draining from the Congo wetland, and to determine the source of the water. We find that the amount of water annually filling and draining the Congo wetlands is 111 km^3, which is about one-third the size of the water volumes found on the mainstem Amazon floodplain. Based on amplitude comparisons among the water volume changes and timing comparisons among their fluxes, we conclude that the local upland runoff is the main source of the Congo wetland water, not the fluvial process of river-floodplain water exchange as in the Amazon. Our hydraulic analysis using altimeter measurements also supports our conclusion by demonstrating that water surface elevations in the wetlands are consistently higher than the adjacent river water levels. Our research highlights differences in the hydrology and hydrodynamics between the Congo wetland and the mainstem Amazon floodplain.

1. Introduction

The Congo Basin is the world's third largest in size (~3.7 million km^2), and second only to the Amazon River in discharge (~40,200 m^3 s^{-1} annual average). The impact and connections of this hydrologic flux with the region's climate, biogeochemical cycling, and terrestrial water storage, especially in wetlands, is of great importance. For example, the extent of the differences in chemistry, seasonality, rate and volume of water input to the floodplain and wetland systems from upland runoff, direct rainfall and mainstem flooding are likely to supply substantially different amounts of nutrients and other solutes (Melack & Engle, 2009). However, the hydrological dynamics of seasonally flooded wetlands and floodplains remains poorly quantified through ground observations, satellite observations or modeling. As a consequence, estimates of the magnitude of other processes driven by such dynamics, such as methane emissions from flooded wetlands that form a significant contribution to global atmospheric methane, also cannot be well estimated. Given the vast size and remote location of the Congo Basin, satellite-borne observations provide the only viable approach to understanding the spatial and temporal distributions of its water balances.

Recently, Alsdorf et al. (2010) have estimated the amounts of water filling and draining from the mainstem Amazon floodplain using data from the Gravity Recovery and Climate Experiment (GRACE) and other satellite measurements. They showed that the majority of water on the mainstem Amazon floodplain is derived from the river with a much less amount from local upland runoff. However, there has been no attempt to estimate the Congo wetland water storage and its flux. In this study, we use satellite-borne observations to suggest a baseline measurement of these storages and fluxes by examining 1) the amount of water stored and drained from the Congo wetland, and 2) whether the water comes from rivers or adjacent upland areas.

We use total storage change in the form of equivalent water height (EWH) change (Wahr et al., 1998) from the GRACE measurements (Tapley et al., 2004), precipitation (P) estimates from the Global Q2

* Corresponding author at: School of Earth Sciences, The Ohio State University, 275 Mendenhall Laboratory, 125 South Oval Mall, Columbus OH 43220 USA. Tel.: +1 614 292 2269.
E-mail address: lee.2444@osu.edu (H. Lee).
[1] Now at Department of Civil and Environmental Engineering, University of Houston, Houston, TX, USA.
[2] Now at Jet Propulsion Laboratory, California Institute of Technology, Pasadena, CA, USA.

0034-4257/$ – see front matter © 2011 Published by Elsevier Inc.
doi:10.1016/j.rse.2011.08.015

Precipitation Climatology Project (GPCP; Adler et al., 2003), evapotranspiration (ET) estimates from the Hillslope River Routing (HRR) model (Beighley et al., 2009), water elevation changes from Environmental Satellite (Envisat) altimeter measurements, and hydrological maps from HydroSHEDS (Lehner et al., 2008). Measurements of inundated area are made from a combination of (1) the Japanese Earth Resources Satellite-1 (JERS-1) Synthetic Aperture Radar (SAR) mosaics developed by the Global Rain Forest Mapping project (GRFM), (2) the Shuttle Radar Topography Mission (SRTM) Digital Elevation Model (DEM), and (3) Moderate-resolution Imaging Spectroradiometer (MODIS) mosaics (Jung et al., 2010a). Unfortunately, we have no available contemporaneous in situ discharge or water stage measurements. We combine these satellite-based measurements to: (1) estimate the wetland storage changes in four regions along the Congo mainstem and its major tributaries, and (2) determine whether the water comes from rivers or adjacent upland areas.

The methods presented here are improved compared to the previous study over the Amazon Basin (Alsdorf et al., 2010) because 1) HydroSHEDS is used to estimate the upland area that contributes directly to the wetland instead of using a ratio between estimates of upland area compared to the wetland area; 2) more realistic ET estimates are used instead of a single number representing the whole basin; and 3) a hydraulic analysis from altimeter measurements is also presented. We also use a longer time span (6 years compared to 2.5 years) of GRACE data.

2. Methods

2.1. Study area

We select four 3°×3° study regions to cover the wetlands of the Congo River mainstem and its major tributaries (Fig. 1). Study region 1 includes the Ubangi River (~3800 $m^3\,s^{-1}$ annual discharge, Laraque et al. (2001)), which is the largest right-bank tributary of the Congo mainstem. Study region 2 includes the Sangha River (~1600 $m^3\,s^{-1}$ annual discharge, Laraque et al. (2001)) and represents the majority of the northern tributary wetlands. Study regions 3 and 4 include eastern and southern tributaries, respectively. The box size is chosen based on the limit of the spatial resolution of GRACE which is determined from the maximum degree ($n_{max}=60$) of the Stokes coefficients.

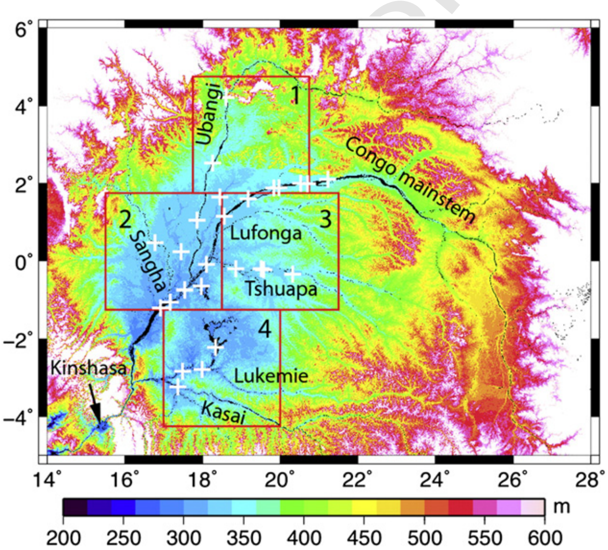

Fig. 1. Locations of four 3°×3° study regions in the Congo Basin. Background shows topography from the SRTM C-band DEM. Intersections between Envisat altimeter and the Congo River are indicated with "+".

2.2. Wetland storage changes from satellite measurements

Total storage changes for a given area, ΔS, are a summation of the storage changes in wetlands (ΔS_w), rivers (ΔS_r), groundwater (ΔS_g), and soil moisture (ΔS_{sm}):

$$\Delta S = \Delta S_w + \Delta S_r + \Delta S_g + \Delta S_{sm}. \quad (1)$$

Measurements from GRACE provide ΔS in terms of anomalies with respect to a mean total storage value. We processed the Release 4 (RL04) Center for Space Research (CSR) GRACE Level 2 (L2) data product (Bettadpur, 2007) from January 2003 to December 2008. To reduce the GRACE longitudinal stripes associated with correlations among even or odd degree Stokes coefficients at resonant orders (Swenson & Wahr, 2006), decorrelation based on Duan et al. (2009) was used. We also applied smoothing using a 3-degree Gaussian filter (Guo et al., 2010). EWHs are computed at 1°×1° grid spacings, and spatially averaged over each study region. Finally, total storage anomalies are obtained by multiplying the EWHs by the box area. More details on the GRACE measurements are provided in Section 3.1.

The channel storage anomalies are estimated by multiplying water stage anomalies, obtained from the Envisat altimeter, with open channel areas estimated from the classification of GRFM image data (Table 1, see discussion below). The Envisat Geophysical Data Records (GDRs) contain 35-day repeat, 18-Hz data (twenty-measurements-per-frame), which corresponds to a ground spacing of approximately 350 m. The GDRs include range measurements from four different retracking algorithms. In this study, we use the retracked measurements from the ICE-1 retracker (Bamber, 1994), which generally Q3 performs well over inland water bodies (Frappart et al., 2006; Lee Q4 et al., 2010). The water stage anomalies over the intersections between the altimeter and the open water bodies are averaged for each tributary, and are then multiplied by the corresponding channel areas.

We use 2.5°×2.5° GPCP monthly merged precipitation rates $P(t)$ (Adler et al., 2003), and create anomalies by subtracting a linear fit, $\bar{P}$, to the integrated sum of $P(t)$ for each study region (see Alsdorf et al., 2010 for details). The slopes of the linear-fit lines represent six-year mean precipitation values, as summarized in Table 1. The GPCP data is derived partly from infrared and microwave satellite measurements, and it should be noted that, as stated in Beighley et al. (2011), there is a discrepancy between various satellite derived precipitation datasets over the Congo Basin in terms of their magnitudes, especially in equatorial regions, which correspond to study regions 2 and 3 in this study. For ET, we use model-based estimates from HRR. It is the sum of wet canopy evaporation, dry canopy transpiration and evaporation from saturated soil surfaces based on the potential ET using Penman–Monteith indirectly through the temperature-based method of estimating its data sources (see Beighley et al., 2009, 2011 for details). The ET rates over each Pfafstetter Level 4 sub-divisions are averaged for each of the four study regions ($\bar{E}$) (Table 1). This Pfafstetter discretization frame-work is a natural system, based on topographic subdivision of the land surface and the resulting topology of the hydrographic network (Verdin & Verdin, 1999). Each level of discretization results in 9 sub-divisions (i.e., 4 tributaries and 5 local contributing areas to the

Table 1
Hydrologic and geomorphic characteristics of each study region.

	Region 1	Region 2	Region 3	Region 4
Upland (km^2)	83,605	42,905	55,297	58,587
Wetland (km^2)	28,052	68,596	56,360	52,914
Channels (km^2)	1058	3990	502	2766
Annual P ($m\,year^{-1}$)	1.44	1.53	1.87	1.71
Annual ET ($m\,year^{-1}$)	0.90	1.01	1.06	0.92
Contributing area (km^2)	121,330	151,596	152,789	141,728

main channel). The ultimate number of sub-areas is $9^{\text{Level Number}}$, but often less than that due to lack of network resolution at higher levels. The Congo Basin was ultimately delineated to Pfafstetter level 4 using a threshold area of ~8.1 km^2 which resulted in 5498 model units (i.e., sub-divisions) with a median model unit drainage area of 670 km^2 and a mean hillslope length of 5.4 km. Anomalies of P − ET are estimated to be:

$$P-ET = \left(P(t)-\bar{P}\right) \times \frac{\bar{P}-E}{\bar{P}}. \qquad (2)$$

The P − ET anomalies are used to estimate the runoff from the local uplands (Section 3.2).

In this study, we assume that groundwater changes associated with the shallow water table (ΔS_g) are driven by P − ET. These changes are assumed to be negligible beneath wetland areas that do not drain, i.e., the water table is assumed to be consistently at the surface in wetlands that contain water from year to year. P − ET varies seasonally and is expected to account for water table variations in the upland areas of each 3°×3° box. Similarly, we assume that P − ET is forcing any soil moisture variations (ΔS_{sm}). Thus, our estimates of P and ET are used, below in Section 3.2, to account for ΔS_g and ΔS_{sm}.

The Congo interfluvial wetlands cover a variety of vegetation and hydrogeomorphic environments. Most of the Congo classifications have been developed based on vegetation type and forest density (e.g., Hansen et al., 2008; Laporte et al., 1995), whereas few classification schemes have focused on flooding in the wetlands (Bwangoy et al., 2009). In this study, we use the hydrogeomorphic flood classification of Jung et al. (2010a).

3. Results and discussions

3.1. GRACE measurements over the Congo Basin

The Congo River is the only major river to cross the equator twice. In doing so, the basin lies in both the Northern and Southern Hemisphere such that it receives year-round rainfall from the migration of the Inter-Tropical Convergence Zone (ITCZ). After the north has its wet season in July–September, the ITCZ moves south and the remainder of the basin receives large amounts of rain. Fig. 2 shows the spatial variations in the storage changes from the CSR GRACE data after decorrelation and smoothing. It can be seen that the positive anomaly in September 2006, which is present outside of the Congo Basin, becomes stronger as it moves southward and into the basin. Likewise, the positive anomaly observed in the southeastern part of the basin in January 2007 becomes stronger and widely spread over the southern boundary of the Congo Basin. This spatial pattern of the storage changes is different from that over the Amazon Basin, where the strongest positive or negative annual water storage anomalies are observed to be centered inside the basin (e.g., Alsdorf et al., 2010; Han et al., 2005).

We also examine the basin-averaged time series of EWH anomalies obtained using four different GRACE data products (from CSR, Jet Propulsion Laboratory (JPL), GeoForschungsZentrum (GFZ), Institut für Geodäsie und Geoinformation (ITG)) using equivalent decorrelation and smoothing (Fig. 3 (top)). They generally agree in terms of their annual increases and decreases in the time series. In addition, all of them show a drying trend until 2006, and then a sharp increase at the end of 2006. However, there are important differences in their amplitudes. There are at least 1 cm EWH differences among the GRACE products; for example, the CSR and ITG solutions differ by at least 1 cm during the last two months of 2005. If we convert this 1 cm EWH difference to streamflow by multiplying it by the basin area (3.7 million km^2) and dividing it by the time duration, we get about 7000 m^3 s^{-1}. As a comparison, this approximately corresponds to the mean annual discharge of the Ohio River in the United States. Moreover, there are at least 5 cm EWH differences between the CSR and JPL solutions that last about 5 months in the first half of 2008. If we again convert this to discharge, we get approximately 14,000 m^3 s^{-1} which corresponds to more than one-third of the Congo River mean annual discharge. It also corresponds to about three-quarters of the Mississippi River discharge. This is a significant difference: note that the Congo and Mississippi River basins are similar in size. Furthermore, the four different GRACE products do not produce the same errors year after year. For example, in the first half of 2006, the JPL solution has generally less EWH values than the CSR solution, but in the second half of 2006 when the trough occurs, the CSR solution values are less than the JPL values. This can be widely observed every year among all of the GRACE products. Overall, the discrepancy among the GRACE products has important implications for Congo hydrology. In addition to different data processing methods and models adopted at different institutes, these disagreements may also be due, in part, to the movement of ITCZ and the consequent leakage of strong signal from outside of the basin (e.g., the strong positive anomaly in September 2006) or from inside of the basin (e.g., the strong positive anomaly in May 2007). This leakage is due to the truncated spectral degree (e.g., $n_{max} = 60$) in the GRACE gravity field solutions and to post-processing smoothing. The leakage phenomenon can occur at all scales including the finest spatial resolution possible with GRACE.

Recently, in the GRACE science community, there has been an effort to use global simulations of water storage variations when

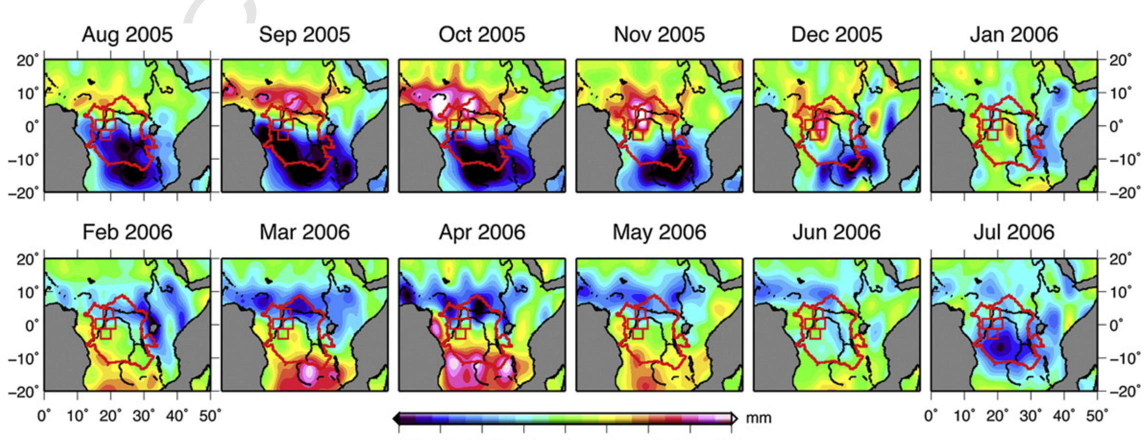

Fig. 2. Monthly Equivalent Water Height (EWH) anomalies from the CSR GRACE product after decorrelation and 3-degree radius Gaussian smoothing. The Congo Basin is shown with a red outer boundary. Red rectangles indicate our study regions. (For interpretation of the references to color in this figure legend, the reader is referred to the web version of this article.)

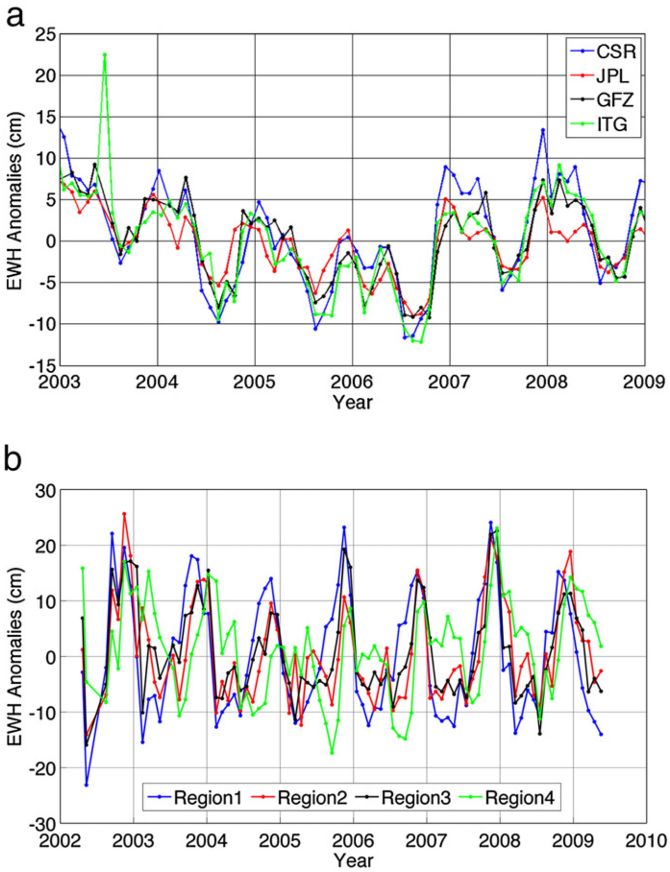

Fig. 3. (top) Comparison among GRACE EWH anomalies over the entire basin after equivalent decorrelation and smoothing. (bottom) Comparison among EWH anomalies over the study regions from CSR GRACE data.

restoring the signal loss in GRACE, which is caused by smoothing. It has been proposed to estimate scale factors, by comparing the unfiltered model time series with the filtered model simulations, to partially correct for the signal attenuation. We have examined the original filtered basin-averaged time series with the scaled time series (data courtesy, S. Swenson) from CSR GRACE data. The scale, computed using the Community Land Model (CLM), averaged over the Congo Basin is 1.2, and thus the scaled time series has a slightly lower amplitude than the smoothed time series. This scale is a simple temporally constant number, intended to depend on the statistical characteristic of the model-simulated storage variations. This approach assumes that errors in the global hydrologic model are spatially and temporally randomly distributed and thus do not introduce a bias in the scaling factor. It is also not entirely clear that a model should be used to correct a measurement, especially in the case of the Congo Basin where model errors are less well-known compared to other regions such as the United States. Moreover, the scaled EWH anomalies cannot resolve the issue of discrepancy among the GRACE products. Therefore, in this study, we do not attempt to correct the leakage error or restore the signal loss due to the smoothing. Rather, we treat the differences among the GRACE products as the error of our storage change estimates.

We now compare the EWH anomalies over our four study regions (Fig. 3, bottom) to examine whether the 3°×3° box size is appropriate and if the storage changes among them can be distinguished. From Fig. 3 (bottom), the EWH anomalies in region 4 are clearly different from the other three regions in terms of their timing and amplitudes. For example, in 2004 region 4 has a trough in August whereas it occurred in February over the other regions. Region 4 also has the smallest peak in December compared to the other regions. Although the timing among regions 1–3 appears to agree, there are differences in anomaly amplitudes. For example, there are about 13 cm EWH differences between regions 1 and 2 during July–September 2006. Converting this difference to river discharge, yields about 3000 $m^3\,s^{-1}$. As another example, about 9 cm EWH differences, lasting about three months at the end of 2005, correspond to about 2000 m^3s^{-1} of streamflow and can be observed between regions 2 and 3. In general, the amplitudes and occasionally the timing of the major peaks and troughs are different among the study regions. This distinction supports our choice of the box size and the resultant wetland volume.

3.2. Wetland water volume change and its flux

We observe from Fig. 4 that the total storage anomalies from GRACE, P − ET anomalies, and river storage anomalies within a given study region are well timed with each other. However, in terms of amplitudes, the river channel storage anomalies are significantly less than the GRACE anomalies, which suggests that storage changes in rivers account for little of the total storage anomalies (note that river anomalies are multiplied by 5, 10, or 20). The P − ET anomaly amplitudes are significantly greater than those of the rivers and typically less than the total storage anomaly amplitudes, which suggest that P − ET accounts for an important fraction of the GRACE measured total volume change. Thus we concluded that hydrological processes associated with P − ET (e.g., runoff) are significant contributors to the total storage change observed in each 3°×3° study region and that in-channel fluvial processes are not significant contributors.

The wetland storage anomalies have two contributors, which are (1) direct precipitation on the wetlands as well as runoff supplied to the wetlands from the surrounding uplands, and (2) water exchanged between the wetlands and the adjacent river channels. It should be noted that the groundwater contribution to the wetland water levels is considered in the upland P − ET runoff because the groundwater is controlled by the infiltration of rainfall. The volumes of runoff from the local uplands and direct rainfall on the wetlands can be estimated by multiplying P − ET with the contributing area or with the inundated area, respectively. The land areas contributing to the wetlands are computed using the following procedures. First, flow directions from HydroSHEDS are obtained to determine flow accumulation and the associated drainage network. Next, we assume that major rivers have width greater than 100 m. This threshold is chosen based on the resolution of the GRFM mosaic, which is used to extract channel areas and to compute the river storage changes in Section 2.2. Based on the relationship between the channel width and the upstream drainage area ($w(m)=0.438\ A_u(km^2)^{0.592}$, Beighley et al., 2011), this 100 m threshold approximately corresponds to rivers with drainage areas larger than 10,000 km^2. We remove these major rivers and their contributing areas from the flow direction grid. Thus, we distinguish the contribution of large river drainage areas from the wetland drainage areas. Then, we extract the wetland pixels for each study region using the classification map (Jung et al., 2010a). Finally, we delineate the area that drains to each wetland pixel for each study region (Fig. 5 and Table 1). Essentially, the fraction of contributing area that is outside of each 3°×3° study region is connected with streams having a drainage area smaller than 10,000 km^2 and that drain directly to a wetland pixel. To further examine whether the 100 m channel width is a reasonable number to distinguish between the contributing areas that flow to the wetlands and the contributing areas that flow to the major rivers, we tracked discharges for all of the rivers which have the contributing areas larger than 10,000 km^2 and that flow into our study regions (red lines in Fig. 5). As summarized in Table 2, we used the HRR model to estimate these discharges during the period 2003–2008 (Beighley et al., 2011). The mean annual discharge for all of the major rivers from a unit contributing area is estimated at 0.016 $m^3\,s^{-1}\,km^{-2}$. For a drainage of 10,000 km^2, this corresponds to 160 $m^3\,s^{-1}$ of discharge. So, the

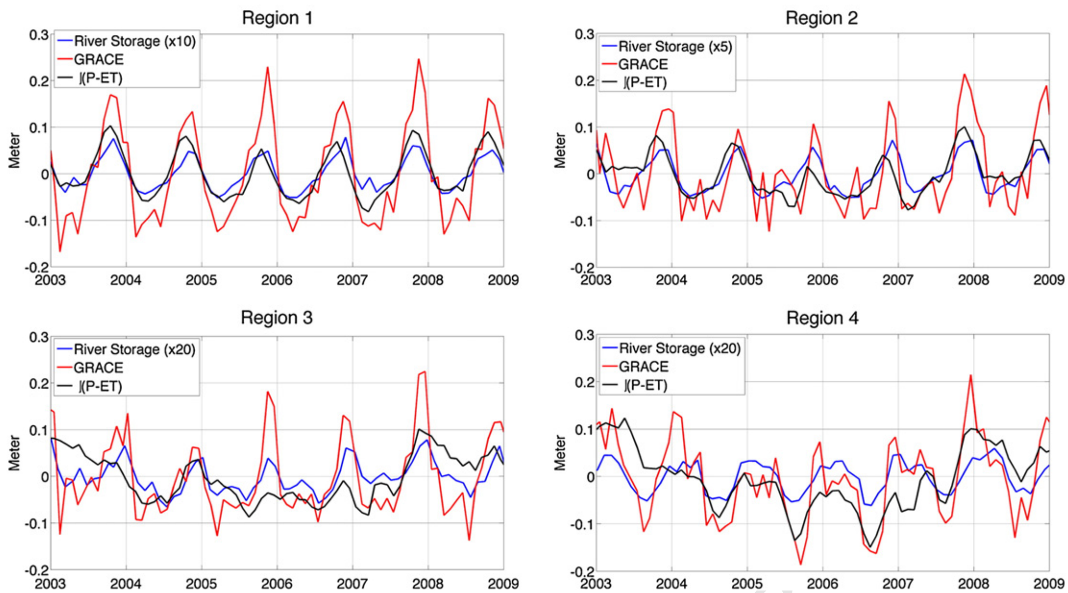

Fig. 4. Time series of satellite-based measurements of Congo hydrology for each study region. Red lines represent EWH anomalies from CSR GRACE data, and black lines are P − ET anomalies. Blue lines show river storage anomalies, and they are multiplied by 5, 10, or 20 for visual clarity. The river storage anomalies in this plot are generated by weighted averages of river stage anomalies with ratios between the channel area and the box area as the weights. (For interpretation of the references to color in this figure legend, the reader is referred to the web version of this article.)

100 m river width threshold (or 10,000 km^2 of contributing area) leads to rivers having a discharge greater than 160 $m^3\ s^{-1}$ and which do not directly flow into the wetlands.

Fig. 6 shows a comparison of water volume anomalies for the wetlands, rivers, and local upland runoff. In each of the four plots, the amplitudes of the river storages are negligible compared to the GRACE and P − ET anomalies. We suggest that this amplitude is not sufficient to supply any significant water volumes that would sufficiently account for the storage changes measured by GRACE or estimated by P − ET. We further explore this concept, i.e., the negligible amount of fluvial exchange between the wetlands and main river channels, in Section 3.3, below. Instead of river supply, the other potentially significant supply of water to the wetlands is runoff from the surrounding uplands and rainfall directly on the wetlands. The P − ET runoff volume anomalies agree well with the GRACE wetland volume anomalies in terms of timing and amplitude in region 1 and reasonably well in region 4. In region 2, there is a large discrepancy in their amplitudes in 2003 and 2004. However, both the GRACE and P − ET anomalies show similar trends throughout the six years time period. The P − ET runoff volume anomalies and the GRACE wetland volume anomalies both reveal a dry

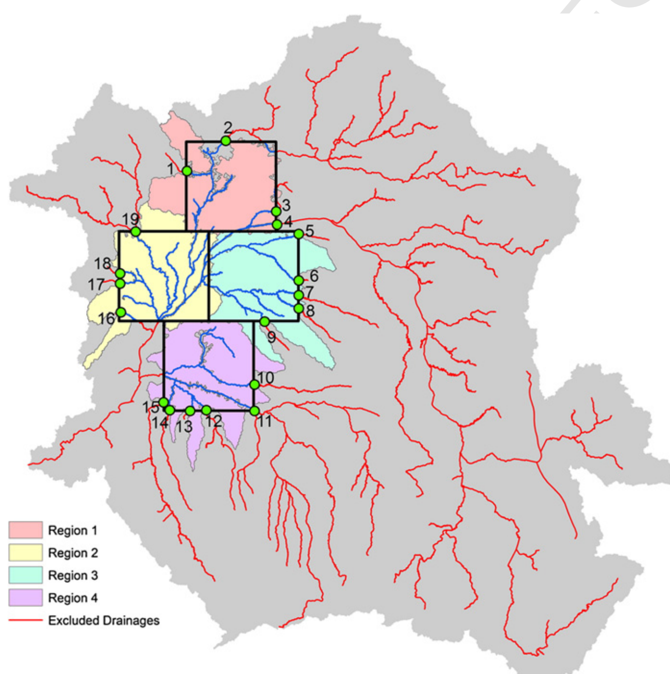

Fig. 5. Colored boundaries represent the contributing land area draining to the wetlands in each study region with the corresponding major rivers (i.e., widths greater than 100 m or contributing areas larger than 10,000 km^2; shown as red lines) and their drainage areas excluded from the study regions; see Table 2 for the hydrologic characteristics of the 19 excluded drainages. (For interpretation of the references to color in this figure legend, the reader is referred to the web version of this article.)

Table 2
Summary of the hydrologic characteristics for the major rivers which have contributing areas greater than 10,000 km^2 based on simulation results from the HRR model for the period 2003–2008.

ID	Study region ID	Contributing area (km^2)	Annual discharge ($m^3\ s^{-1}$)	Annual discharge per unit area ($m^3\ s^{-1}\ km^{-2}$)
1	1	31,270	429	0.014
2	1	479,839	5527	0.012
3	1	45,642	675	0.015
4	1	1,348,434	18,686	0.014
5	3	16,073	209	0.013
6	3	21,639	322	0.015
8	3	39,284	419	0.011
9	3	18,809	343	0.018
10	4	47,199	720	0.015
11	4	453,653	6587	0.015
12	4	65,691	1279	0.019
13	4	25,752	551	0.021
14	4	35,334	753	0.021
15	4	136,132	2187	0.016
16	2	10,547	283	0.027
17	2	14,145	221	0.016
18	2	13,713	190	0.014
19	2	158,137	2825	0.018
				Mean: 0.016

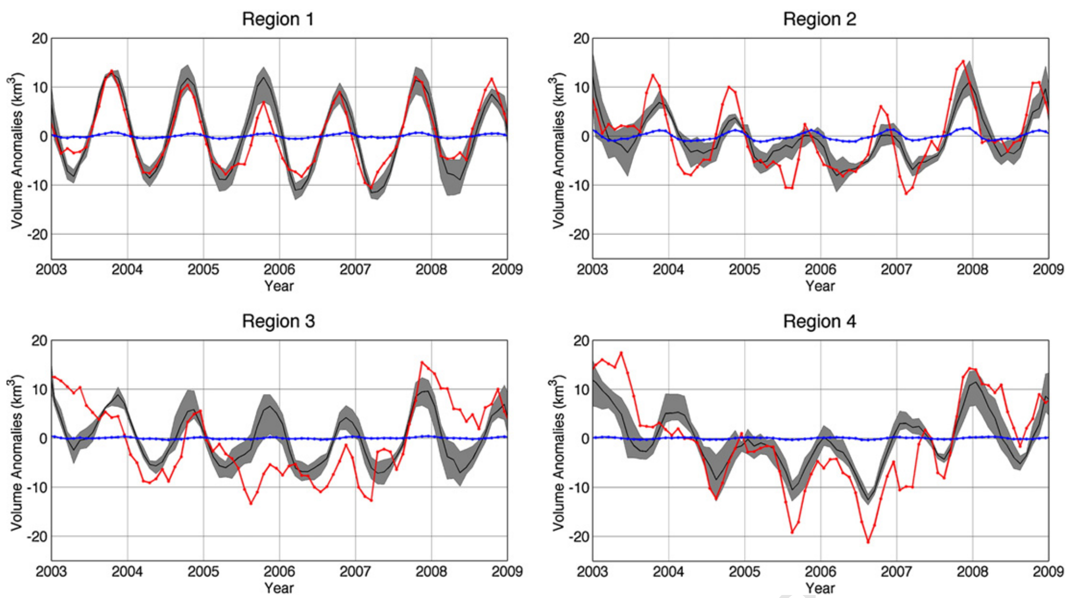

Fig. 6. Water volume anomalies of river (blue) and runoff (red). The shading illustrates the range wetland water volume anomalies estimated using CSR, JPL, GFZ, and ITG GRACE solutions. The black solid line indicates the mean of the four estimates. (For interpretation of the references to color in this figure legend, the reader is referred to the web version of this article.)

season in 2005 and a rather wet season in late 2007. Essentially, both data show somewhat wetter years in 2003 and 2004, dryer years in 2005 and 2006, and returning to wetter years in 2007 and 2008. In region 3, we observe that the timing of volume increases and decreases do not generally agree between the wetland and the runoff anomalies, although they both show an excessive volume of water in 2007. In summary, region 1 annually fills and drains about 20 km^3 to 25 km^3 of water each year whereas regions 2, 3 and 4 fill and drain about 10 km^3 to 20 km^3.

The differences observed in regions 2 and 3 may be due to problems with satellite rainfall products in the equatorial region. For example, Beighley et al. (2011) used three satellite derived precipitation datasets (TRMM, CMORPH, PERSIANN) to drive the HRR model throughout the Congo Basin. The results, which were compared to historical discharges, Envisat altimetry measurements and GRACE water storages, show that satellite precipitation products provide unreasonably high rainfall for specific time periods (e.g., all three in Oct–Nov; only CMORPH and PERSIANN in Mar–Apr) in the equatorial regions. These findings are also consistent with previous studies that found large discrepancies between gage and satellite precipitation over equatorial regions of Africa (e.g., McCollum et al., 2000; Nicholson et al., 2003). Although additional research is needed to resolve this issue, one possible cause may be related to the significant level of lightning activity in the region (Williams and Satori, 2004).

The rates of wetland filling and draining (Fig. 7) are computed by taking the temporal derivative of the storage anomalies in Fig. 6 (Alsdorf et al., 2010). Regions 1 through 4 have about $\pm 1000\ m^3\ s^{-1}$ to $2000\ m^3\ s^{-1}$ of wetland discharge during flooding and draining. Summing the maximum and minimum wetland flux rates for all four regions yields $\pm 6400\ m^3\ s^{-1}$ during flooding and emptying, or $\pm 16\%$

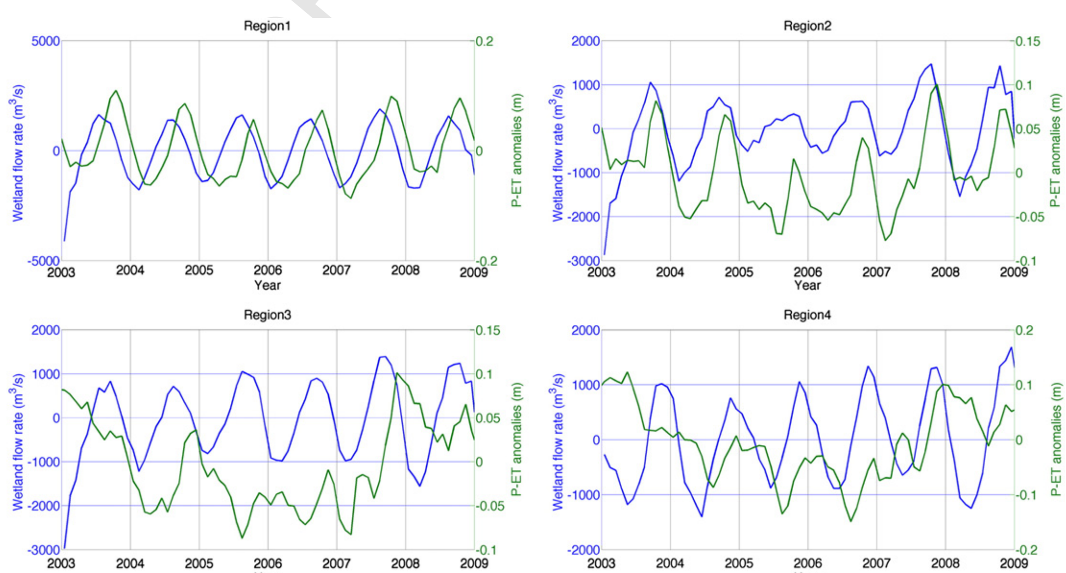

Fig. 7. Wetland flow rates (blue, left Y-axis) and P − ET anomalies (green, right Y-axis). (For interpretation of the references to color in this figure legend, the reader is referred to the web version of this article.)

of the mainstem annually averaged discharge, i.e., 40,000 $m^3\ s^{-1}$ at the historic Kinshasa gage (Fig. 1). Summing the maximum volumes for all four regions yields 111 km^3 of water stored and subsequently emptied each year from the Congo wetland. This corresponds to only about 8% of the total volume of water annually discharged from the Congo.

The timing of wetland filling (when the flux becomes positive from negative) and draining (when the flux becomes negative from positive) can be compared with the timing of increasing and decreasing of P − ET to examine a temporal connection between them. Note that in Fig. 7 we are comparing wetland flow rates derived from GRACE (blue line) to changes in P − ET (green line). In regions 1, 2, and 4, P − ET is always increasing when the wetland flux rates change from negative to positive, i.e., from draining to filling. P − ET therefore always comes before the wetland filling, and thus from a temporal perspective, the wetland infilling starts with the P − ET runoff from the surrounding uplands. On the other hand, when the wetland flux rates switch from positive to negative, P − ET is always on the decreasing limb of the annual rainfall. This again is expected where the wetland receives the majority of its water from upland runoff.

3.3. Hydraulic analysis using altimeter measurements in the Congo and Amazon basins

Our interpretation that the Congo wetlands receive the majority of their water from upland runoff as opposed to exchange with adjacent major tributaries as suggested by comparisons of GRACE anomalies with P − ET anomalies, is also supported by Envisat altimeter observations. The water elevation changes over the wetland regions, which have low topographic relief and higher radar backscatter, are generated and compared with the water elevation changes over adjacent river channels (for example, red circles in Fig. 8(a)). The vertical datum of both river and wetland water elevations is referenced to the Earth Gravitational Model 2008 geoid (EGM08; Pavlis et al., 2008). Top panels of Fig. 9(a) and (b) show the surface height profiles along the altimeter tracks obtained from several altimeter samplings over the red circle regions in Fig. 8(a). We observe fluctuations in the water elevations of the Congo mainstem and its adjacent wetlands in each altimeter overpass. We then generate water elevation change time series by combining successive overpasses. It should be noted that the wetland regions closest to the river channels along the tracks are selected and compared with the river water fluctuations. As shown in the bottom panels of Fig. 9(a) and (b), the range in wetland water levels is small compared to the river. Moreover, the wetland water topographic elevations are overall between 0.5 and 2.5 m above the river, i.e., the wetland water levels are always greater than the river. Clearly, the river cannot flow "uphill" into the wetlands. Therefore, the wetlands do not receive water from the adjacent major tributaries or mainstem Congo River and instead can only supply water to the rivers. While these observations are necessarily local to the red-circled areas in Fig. 8(a), they support the previous interpretation which used GRACE observations to suggest that the local upland runoff is the main source of the Congo wetland water. We have investigated several more altimeter overpass locations (black-circled in Fig. 8(a)), where the altimeter footprint allows delineation of wetlands and rivers, and nearly all locations demonstrate that wetland water elevations are consistently higher in elevation than the adjacent river. It may be argued that the river channel at the location of the altimeter transect is located further downstream than the wetland. In this case, the wetland water levels can always be higher than the river, and it does not necessarily indicate that the river waters cannot flow into the wetlands. However, this is true only if there are abundant floodplain channels that connect the wetlands to the adjacent river channel. Jung et al. (2010b) highlighted the fundamental differences in the water level changes between the Amazon and Congo wetlands, using Interferometric Synthetic Aperture Radar (InSAR) measurements, due to differences in the connectivity of the floodplain-river systems. The result suggests that connectivity of the Congo River to the interfluvial wetland area is limited, compared with the Amazon.

To further demonstrate that altimeter measurements are a hydraulic indicator of the direction that water can or cannot flow, we also examine Envisat altimeter measurements over the Amazon Basin. These serve as a comparison to the Congo. We generate the time series of water elevation changes over the Amazon mainstem (Solimoes River) and its adjacent floodplain (Fig. 9(c)). We note that the water levels at mid-rising stage in the floodplain are lower than the river, but the low water levels are almost identical. This implies that the water is flowing down the hydraulic slope from the river to the floodplain during mid-rising stage. Moreover, in nearly every year, the river clearly rises before the floodplain. These timings, in combination with the elevations noted

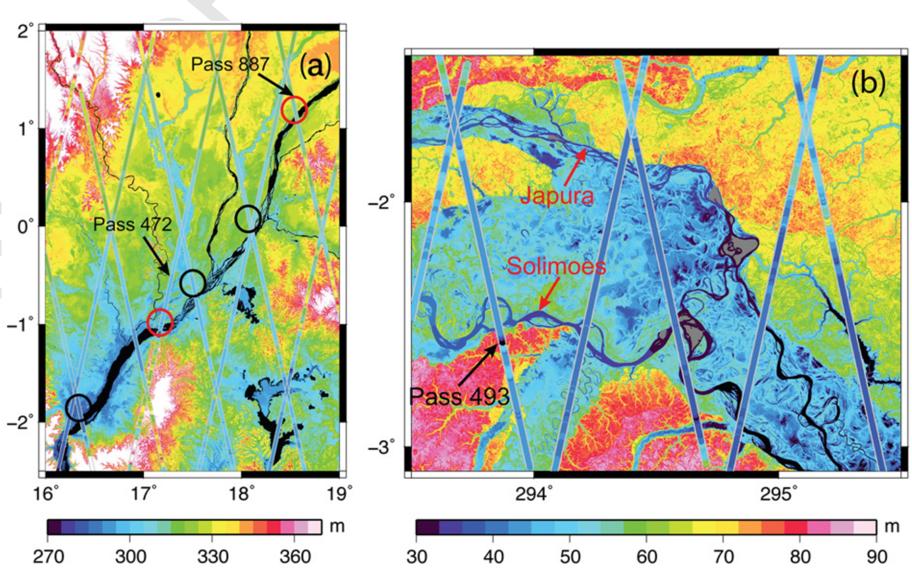

Fig. 8. Color-coded lines represent Envisat 18-Hz ICE-1 retracked surface heights, referenced to EGM96 geoid, over (a) the Congo Basin from cycle 12 (December 2002), and (b) the Amazon Basin from cycle 18 (August 2003). Background is SRTM DEM. (For interpretation of the references to color in this figure legend, the reader is referred to the web version of this article.)

Please cite this article as: Lee, H., et al., Characterization of terrestrial water dynamics in the Congo Basin using GRACE and satellite radar altimetry, *Remote Sensing of Environment* (2011), doi:10.1016/j.rse.2011.08.015

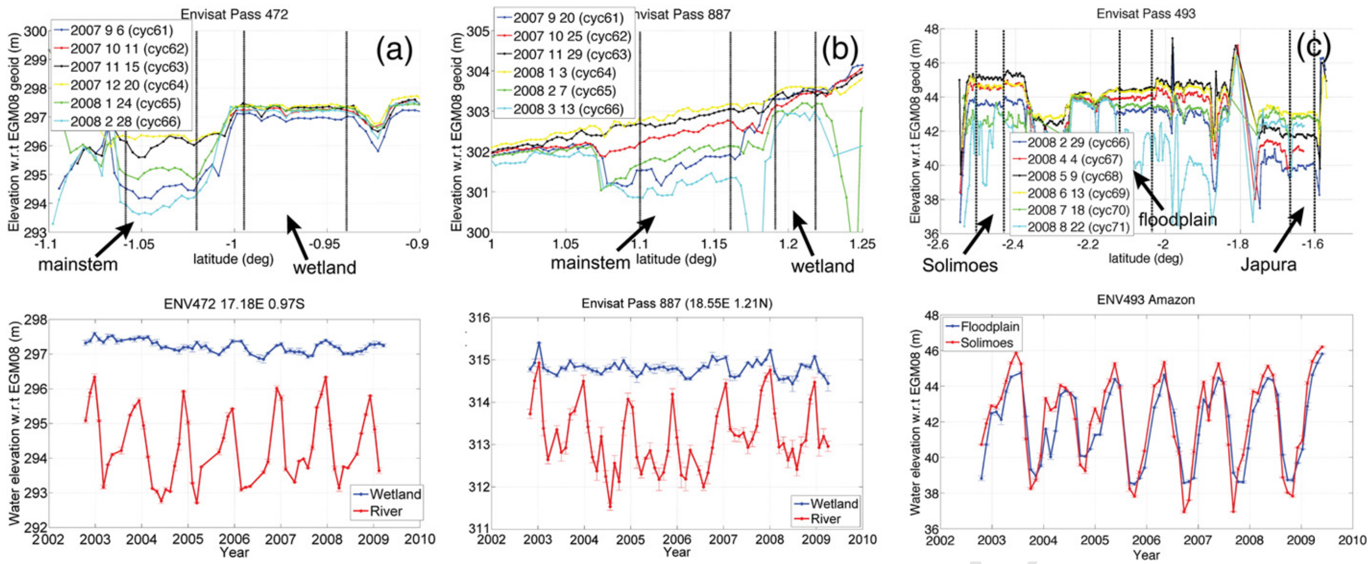

Fig. 9. Water level fluctuations over the Congo mainstem and its adjacent wetlands along (a) Envisat passes 472 and (b) 887 over the red circle regions in Fig. 8. Water level variations over the Amazon River and its floodplain are shown in (c). They are referenced to the EGM08 geoid. (For interpretation of the references to color in this figure legend, the reader is referred to the web version of this article.)

above, imply that the Amazon river is flowing into the floodplain. We also observe that the river has a "shoulder" in the mid-rising times of every year where the water level stops rising, or at least slows its rising before rapidly rising again. The floodplain shows a similar shoulder. This further suggests that the floodplain is responding to the river. These observations indicate that the floodplain of the Amazon mainstem derives its water more from the river, than from the uplands: a conclusion already supported by GRACE observations in Alsdorf et al. (2010).

4. Conclusions

The amount of water annually filling and draining the Congo wetland is large, but only about one-third of the mainstem Amazon floodplain volumes (111 km^3 compared to 285 km^3; Alsdorf et al., 2010). Based on the amplitude comparison among the water volume changes and the timing comparison among their fluxes, we conclude that the local upland runoff is the main source of the Congo wetland water, not the fluvial process of river-wetland water exchange. Delineating whether the water comes from local uplands or from distal places via fluvial transport presumably makes a difference in the sediment supplies and in the carbon and nutrient exchanges. For example, given the hydraulic gradient analysis of Section 3.3, it is unlikely that the Congo wetlands are filled with sediments derived from erosion processes in the Congo headwaters around the western flanks of the East Africa Rift system. Our analysis using altimeter measurements, although they could be local observations considering the vast size of the basins, supports our conclusion, highlighting the difference between the Congo wetland and the Amazon floodplain hydraulics. Our finding is in alignment with Jung et al. (2010b) which concluded that flow patterns in the Congo are less governed by channel connectivity because flooded areas in the Congo are broadly distributed and do not have abundant floodplain channels as in the Amazon.

Although we assumed the contribution of soil moisture and groundwater variation to the total storage change is negligible compared to that of the surface water, further studies are needed to accurately determine the portions of the soil moisture and groundwater changes that account for the total changes in the water balance, compared to the channel and wetland discharges. The HRR hydrologic and hydraulic model (Beighley et al., 2009, 2011) and the CaMa-Flood macro-scale floodplain model (Yamazaki et al., 2011) can help us determine not only those portions, but also simulate the wetland storage changes in the Congo to compare with our results.

References

Adler, R. F., Huffman, G. J., Chang, A., Ferraro, R., Xie, P., Janowiak, J., et al. (2003). The version 2 global precipitation climatology project (GPCP) monthly precipitation analysis (1979–present). *Journal of Hydrometeorology*, *4*, 1147–1167.

Alsdorf, D., Han, S. -C., Bates, P., & Melack, J. (2010). Seasonal water storage on the Amazon floodplain measured from satellites. *Remote Sensing of Environment*, *114*, 2448–2456.

Beighley, R. E., Eggert, K. G., Dunne, T., He, Y., Gummadi, V., & Verdin, K. L. (2009). Simulating hydrologic and hydraulic processes throughout the Amazon River Basin. *Hydrological Processes*, *23*, 1221–1235.

Beighley, R. E., Ray, R. L., He, Y., Lee, H., Schaller, L., Durand, M., et al. (2011). Comparing satellite derived precipitation datasets using the Hillslope River Routing (HRR) model in the Congo River Basin. *Hydrological Processes*, doi:10.1002/hyp. 8045 (published online).

Bettadpur, S. (2007). CSR Level-2 processing standards document for product Release 04. *GRACE 327–742, Center for Space Research, University of Texas at Austin*.

Bwangoy, J. -R. B., Hansen, M. C., Roy, D. P., de Grandi, G., & Justice, C. O. (2009). Wetland mapping in the Congo Basin using optical and radar remotely sensed data and derived topographical indices. *Remote Sensing of Environment*, *114*, 73–86.

Duan, X. J., Guo, J. Y., Shum, C., & van der Wal, W. (2009). On the postprocessing removal of correlated errors in GRACE temporal gravity field solutions. *Journal of Geodesy*, *83*, 1095–1106.

Guo, J. Y., Duan, X. J., & Shum, C. (2010). Non-isotropic filtering and leakage reduction for determining mass changes over land and ocean using GRACE data. *Geophysical Journal International*, doi:10.1111/j.1365- 246X.2010.04534.x.

Han, S. -C., Shum, C., Jekeli, C., & Alsdorf, D. (2005). Improved estimation of continental water storage change from GRACE. *Geophysical Research Letters*, *32*, doi:10.1029/2005GL022382.

Hansen, M. C., Roy, D. P., Lindquis, E., Adusel, B., Justice, C. O., & Altstatt, A. (2008). A method for integrating MODIS and Landsat data for systematic monitoring of forest cover and change in the Congo Basin. *Remote Sensing of Environment*, *112*, 2495–2513.

Jung, H., Alsdorf, D., Lee, H., Trigg, M., & Fewtrell, T. (2010). Hydrogeomorphic flood classification and hydrodynamic modeling of the Congo interfluvial wetlands. *AGU fall meeting abstract*.

Jung, H., Hamski, J., Durand, M., Alsdorf, D., Hossain, F., Lee, H., et al. (2010). Characterization of complex fluvial systems using remote sensing of spatial and temporal water level variations in the Amazon, Congo, and Brahmaputra Rivers. *Earth Surface Processes and Landforms*, *35*, 294–304.

Laporte, N., Justice, C., & Kendall, J. (1995). Mapping the dense humid forest of Cameroon and Zaire using AVHRR satellite data. *International Journal of Remote Sensing*, *16*, 1127–1145.

Laraque, A., Mahé, G., Orange, D., & Marieu, B. (2001). Spatiotemporal variations in hydrological regimes within Central Africa during the XXth century. *Journal of Hydrology*, *245*, 104–117.

Lee, H., Durand, M., Jung, H., Alsdorf, D., Shum, C., & Sheng, Y. (2010). Characterization of surface water storage changes in Arctic lakes using simulated SWOT measurements. *International Journal of Remote Sensing*, *31*, 3931–3953.

Lehner, B., Verdin, K., & Jarvis, A. (2008). New global hydrography derived from spaceborne elevation data. *Eos*, *89*, 93–94.

Please cite this article as: Lee, H., et al., Characterization of terrestrial water dynamics in the Congo Basin using GRACE and satellite radar altimetry, *Remote Sensing of Environment* (2011), doi:10.1016/j.rse.2011.08.015

McCollum, J. R., Gruber, A., & Ba, M. B. (2000). Discrepancy between gauge and satellite estimates of rainfall in equatorial Africa. *Journal of Applied Meteorology*, *39*, 666–679.

Melack, J. M., & Engle, D. (2009). An organic carbon budget for an Amazon floodplain lake. *Verhandlungen — Internationale Vereinigung Limnologie*, *30*, 1179–1182.

Nicholson, S. E., Some, B., McCollum, J., Nelkin, E., Klotter, D., Berte, Y., et al. (2003). Validation of TRMM and other rainfall estimates with a high-density gauge dataset for West Africa. Part I: Validation of GPCP rainfall product and pre-TRMM satellite and blended products. *Journal of Applied Meteorology*, *42*, 1337–1354.

Pavlis, N. K., Holmes, S. A., Kenyon, S. C., & Factor, J. K. (2008, April). An earth gravitational model to degree 2160: EGM2008. Vienna, Austria: EGU-2008 (also see). http://earth-info.nga.mil/GrandG/wgs84/gravitymod/egm2008/index.html

Swenson, S., & Wahr, J. (2006). Post-processing removal of correlated errors in GRACE data. *Geophysical Research Letters*, *33*, L08402, doi:10.1029/2005GL025285.

Tapley, B. D., Bettadpur, S., Ries, J., Thompson, P., & Watkins, M. (2004). GRACE measurements of mass variability in the Earth system. *Science*, *305*, 503–505.

Verdin, K. L., & Verdin, J. P. (1999). A topological system for delineation and codification of the earth's river basins. *Journal of Hydrology*, *218*, 1–12.

Wahr, J., Molenaar, M., & Bryan, F. (1998). Time variablility of the earth's gravity field: Hydrological and oceanic effects and their possible detection using GRACE. *Journal of Geophysical Research*, *103*, 30205–30229.

Williams, E. R., & Satori, G. (2004). Lightning, thermodynamics and hydrological comparison of the two tropical continental chimneys. *Journal of Atmospheric and Solar-Terrestrial Physics*, *66*, 1213–1231, doi:10.1016/j.jastp. 2004.05.015.

Yamazaki, D., Kanae, S., Kim, H., & Oki, T. (2011). A physically based description of floodplain inundation dynamics in a global river routing model. *Water Resources Research*, *47*, W04501, doi:10.1029/2010WR009726.